Mutations in artificial self-replicating tiles: A step toward Darwinian evolution

Feng Zhou[a,1], Ruojie Sha[b], Heng Ni[a], Nadrian Seeman[b,1], and Paul Chaikin[a,1]

[a]Department of Physics, New York University, New York, NY 10003; and [b]Department of Chemistry, New York University, New York, NY 10003

Edited by Oleg Gang, Columbia University, New York, NY; received June 24, 2021; accepted November 2, 2021 by Editorial Board Member Joanna Aizenberg

Artificial self-replication and exponential growth holds the promise of gaining a better understanding of fundamental processes in nature but also of evolving new materials and devices with useful properties. A system of DNA origami dimers has been shown to exhibit exponential growth and selection. Here we introduce mutation and growth advantages to study the possibility of Darwinian-like evolution. We seed and grow one dimer species, AB, from A and B monomers that doubles in each cycle. A similar species from C and D monomers can replicate at a controlled growth rate of two or four per cycle but is unseeded. Introducing a small mutation rate so that AB parents infrequently template CD offspring we show experimentally that the CD species can take over the system in approximately six generations in an advantageous environment. This demonstration opens the door to the use of evolution in materials design.

artificial self-replication | mutation | Darwinian evolution | exponential growth | cross-tile DNA origami

Nature has been very successful in making a wide variety of functional materials, devices, and organisms through natural selection. DNA origamis are convenient starting points for artificial materials evolution. Not only can they be designed to form almost arbitrary shapes (1–6), but also they can be joined programmably with each other to make objects on a larger scale (7–9). Further, they can precisely organize other materials such as nanoparticles (10, 11), nanotubes (12, 13), and enzymes (14). Previously we have demonstrated self-replication, exponential growth, and selection in DNA origami tiles. The basic replication scheme is to template the transfer of structure and information from one generation to the next (15–18). This involves specific recognition of elementary units, organization, and reversible and irreversible binding. However, the initial efforts were to make the system as error-free as possible, and in fact the experiments showed only copies of the seeded patterns. The recognition strands were sufficiently specific that they would only hybridize to their complementary strands ensuring correct templating. It has also been demonstrated that exponential growth with a well-controlled growth rate can be achieved in the DNA origami artificial self-replication system (19, 20). As a start on evolutionary pressure to evolve new and better materials and devices we now want to introduce mistakes, mutations.

Errors, i.e., mutations, can occur in self-replication when we change the recognition strands. The original DNA origami species were self-complementary in the recognition strands sequence. Now we make them self-complementary and almost complementary to the mutated species by using strands that differ by one to five nucleotides between the two species. With the cross-over we should have a mixture of original and mutated species after many replication cycles, similar to the historical example of the peppered moth where the fittest species dominated but neither species went extinct (21).

Here, we report the study of the mutation and evolution of an artificial self-replication system of DNA origami dimer rafts. This represents a first step toward using such mutations toward directed evolution of an artificial system and illustrates some of the basic principles of natural selection. We designed two self-replicating species AB and CD which share the same replication procedure, but with a controllable growth rate. Starting with monomers, A, B or C, D, there is negligible growth of dimers in the absence of AB or CD templating seeds; any dimers that are formed are sterile and do not replicate (19). If we were to introduce an AB seed with no mutation possible then AB would exponentially grow and there would be negligible CD. By introducing a small error (3 bases) in the AB recognition sticky strands (42 bases in total), there was a small chance of ∼3% for the system to mutate templating a CD which can replicate itself effectively, starting a new species. The mutation rate is small, but the mutated nanostructure shares the same replication ability as the original dimer. Although the original dimers are dominant at the beginning of self-replication, after many replication cycles we should have an equal mixture of mutated and original dimers if AB and CD have the same growth rates. In addition, we can create differences in the self-replication rates of AB and CD species and give growth advantage to the CD structures; then, after many replication cycles, the mutated species will take over the system. We can use the functionality of the different species to affect this takeover. Mutation and population domination by the fittest species would amount to natural selection in this artificial system. With an eye toward using this process for directed evolution and the fact that a high mutation rate leads to an Eigen catastrophe (22), or a species does not persist long enough to take advantage of its evolutionary advantage, we have kept the mutation rate low, although not yet as low as

Significance

In nature, mutation is the first step of evolution, where it provides the genetic variation for the natural selection to act. Here we take a system of artificial self-replicating tiles, DNA origami, that exhibit templated reproduction. We can generate a small fraction of mutations by introducing a mismatch in hybridization between parent and daughter. We can modify the origami functionality to affect the growth rate of the mutated species, giving it less or more evolutionary advantage, and to become dominant in several generations. The introduction of mutations into an artificial self-replicating system provides new directions for research into self-assembly processes.

Author contributions: F.Z., R.S., N.S., and P.C. designed research; F.Z. and H.N. performed research; F.Z., R.S., N.S., and P.C. analyzed data; and F.Z., N.S., and P.C. wrote the paper.

The authors declare no competing interest.

This article is a PNAS Direct Submission. O.G. is a guest editor invited by the Editorial Board.

[1]To whom correspondence may be addressed. Email: zfedward1988@gmail.com, ned.seeman@nyu.edu, or chaikin@nyu.edu.

This article contains supporting information online at http://www.pnas.org/lookup/suppl/doi:10.1073/pnas.2111193118/-/DCSupplemental.

Published December 6, 2021.

in living systems. In the present case a low mutation rate is particularly important in that the forward and reverse mutations are equally limiting the final ratio of the species with high and low growth advantage.

Results

The present mutation and evolution experiments are based on the established self-replication procedure illustrated in Fig. 1. We use cross-tile DNA origami with perpendicularly organized DNA helices along the two axes and a characteristic thicker "equal sign" easily observable in an atomic force microscope (AFM) where the two perpendicular halves are joined Fig. 1*A* (7). Reversible "recognition" sticky ends, single-stranded DNA, containing seven nucleotides in each strand, were placed on the vertical arms for temperature-dependent reversible hybridization. Four photo-cross-linkable sticky ends containing 3-cyanovinylcarbazole (^{CNV}K) were placed on one of the horizontal arms for permanently linking complementary A and B cross-tile origamis at a lower temperature (23). The replication process, Fig. 1*B*, proceeds by introduction of parent dimer AB seeds into a suspension of single A and B tiles, lowering the temperature so that A and B tiles assemble above or below AB tiles. The temperature is set such that A and B tiles will not hybridize in suspension. However, when they are attached to the dimer template the y-y′ or z-z′ sticky ends are held in close proximity and their local concentration is increased by ~10^6 and they hybridize. While held cold the sample is illuminated with ultraviolet (UV) light (365 nm) and the horizontal sticky ends are covalently bound by

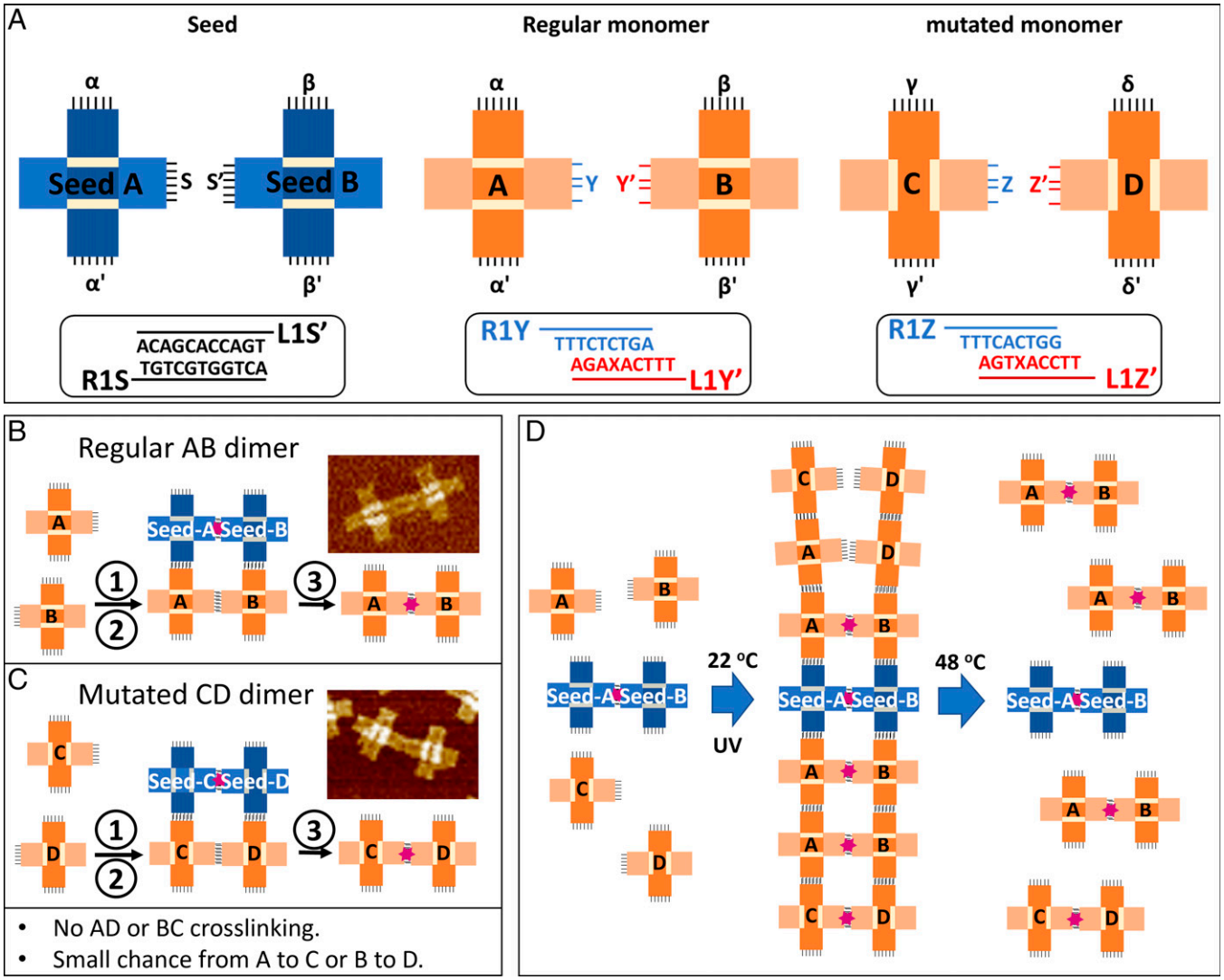

Fig. 1. (*A*) Schematics of DNA origami tiles for litters/ladder self-replication system. The seed A-B dimer is held together by six 11-bp complementary horizontal sticky ends (S and S′). Both A-B and C-D monomers have a unique set of horizontal sticky ends (Y and its complement Y′ for A-B, and Z and its complement Z′ for C-D), where there is a ^{CNV}K (denoted X in the Y′ and Z′ sequences) unit on each of the four strands in Y′ and Z′ (red lines), so no cross-over reaction can happen between A-D or B-C. The seed and monomer A-B contains two sets of six vertical sticky ends (α, β) that extend from the top of the tiles and another two sets of complementary sticky ends (α′, β′) from the bottom of the tiles. The monomer C-D contains two sets of complementary vertical sticky ends (γ-γ′, δ-δ′). α, β differ from γ, δ by a few nucleotides in the sequence design, so there is a small chance for self-assembly of A and C or B and D. Schematics of self-replication of (*B*) seed A-B using A and B monomer and (*C*) seed C-D using C and D monomer. The general replication cycle contains three steps: 1) annealing at 22 °C for the seed-templated self-assembly; 2) exposure to a 365-nm UV LED at 22 °C; and 3) heating to 48 °C to break the vertical sticky end hybridization. The monomers hybridized on one side or two sides of the seed dimer (template) can be photochemically cross-linked to form new dimers. (*Inset*) The AFM images of the dimers show the orientation of "equal sign" to distinguish between the two species. (*D*) Mutation from A-B dimer to C-D dimer during the self-replication. The system starts with an A-B dimer and monomers A, B, C, and D. Mutation in the self-assembly can lead to change of the species during the self-replication.

photo-cross-linking of ^{CNV}K to form the new dimer structure. On heating the daughter dimers are released and form the parent templates for the next generations. On repeated cycles of cooling, UV illumination, and heating the number of offspring dimers grows exponentially. The growth rate is determined both by the thermodynamics of the recognition strands and by the relative concentrations of the monomers and parent dimers. If only half of the monomer vertical arms are functionalized with sticky ends, then the replication rate is less than a factor of 2 per cycle (*SI Appendix*, Fig. S1*A*). However, if both vertical arms are functionalized the parent dimer can nucleate a one-dimensional ladder and in one cooldown, UV cross-linking, and release we can have a litter of offspring and an exponential growth of up to a factor of ∼10 per cycle (20) (*SI Appendix*, Fig. S1*C*).

For the mutation experiments we introduced a new set of self-replicating tiles C and D, with 90° rotation of the tiles and their AFM identifying equal signs, Fig. 1*C*. C and D vertical and horizontal arms are functionalized with different sequences than A and B tiles (Fig. 1*C*). A and C have similar complementary vertical strands, but with a small difference at the end of each strand. Thus, A has a small chance to bind with C, instead of itself, and vice versa. Similarly, B and D have a small probability to bind as compared to B/B (B/B implies B over B) or D/D. In order to simplify the mutation results, the two dimer species share the same ^{CNV}K horizontal sticky ends design but distinct DNA sequences, preventing the photo-cross-linking of AD or BC dimers. As illustrated in Fig. 1*D*, If the system starts with only the AB parent dimer, the AB nucleated ladder would mostly have AB dimer rungs but may contain a small portion of CD rungs. After UV exposure and heating, this produces many new AB dimers and a few "mutated" CD dimers. Note that AD and CB dimers are prohibited by the very noncomplementary cross-linking strands. We can follow the evolution of the dimer species by monitoring the change of ratio between the AB and CD dimers from AFM images, as we repeat replication cycles. We refer to CD dimers as mutations as the sample is seeded only with AB. CD results from unfavored binding of mismatched DNA sticky ends on the vertical arms.

In order to control the mutation rate between AB and CD, we introduced mismatches onto the vertical recognition sticky ends that bind monomers to the parent template. Normally β-strands on the top of B bind to complementary β′-strands on the bottom of another B. However, if the δ′-strands on the bottom of D are almost complementary to β then D will bind to B but with a lower probability than B with B. As shown in Fig. 2*A*, we introduced single mismatches in several recognition vertical sticky ends on D which is mutated from B. We then quantified the effect of changing the number of mismatched recognition strands on the B/D binding using fluorescence resonance energy transfer (FRET). As shown in Fig. 2*B*, the B monomer consisting of the regular DNA sticky ends was hybridizing with the D monomer consisting of the mutated complementary DNA sticky ends with the mismatches. The cy3 on B and cy5 on D form a FRET pair after hybridization and cause the decrease of the emitted light intensity of the cy3 compared to the free-diffusing cy3 in the control sample (*SI Appendix*, Fig. S2). By analyzing the change of the emission light intensity, we can plot the change of the FRET pair composition as temperature is changed, obtaining a melting curve (Fig. 2*B*). The melting curve shifts to lower temperature as we increased the number of mismatched strands in the D monomer. When the fifth mismatch is introduced, the hybridization starts at 23 °C. Since the photo-cross-linking is conducted at 22 °C in our replication process, we study the fraction of B/D dimers for one to four mismatch recognition sticky ends.

We mixed B monomers with two different monomers: B′ monomers with 0 mismatch and the D monomers with zero to four mismatches. During the annealing procedure from 48 °C to 20 °C, B monomers have a higher probability to hybridize with B′ and to form B′/B dimers because of their higher melting temperature, compared to the D that forms the mutated dimer B/D (Fig. 2*C*). With the benefit of the equal-sign design, the regular B/B′ binding could be recognized with the parallel equal sign "|| ||," while the mutated B/D binding had the perpendicular equal signs "= ||." The equal-sign orientation was observed on the AFM, and we measured the hybridization selection by counting the two species after annealing (*SI Appendix*, Figs. S3 and S4). We found that the fraction of mutated BD binding, "= ||," would decrease with more mismatches introduced. We observed a continuous decrease in the fraction of the mutated B/D binding when more mismatches were introduced in the D monomer. With mutated monomers with three mismatches, we obtain 16% mutated binding, B/D ÷ (B/D +B/B) = 0.16. Similarly, for A/C the mutation rate is 16%. Considering that the specific sequence of the ^{CNV}K sticky ends only permits the photo-cross-linking between two regular monomers or two mutated monomers, the mutation rate leading to CD dimers is $\sim 0.16^2/(0.16^2 + 0.84^2) \sim 3.5\%$ for three mismatches in the vertical sticky ends. In the following mutation self-replication experiments, the design for the mutated recognition strands contains three mismatches.

In Fig. 3 we show the results of a mutation experiment in which the growth rates of the two species AB and CD are approximately equal at 3.7 and 3.9 per cycle. In our litter/ladder self-replication systems the growth rate is controlled by the ratio of the number of AB dimers to the number of A and B monomers in each cycle and the number of CD dimers to C and D monomers per cycle. After each cycle the system is divided into two batches; one-third are used to seed the next generation and two-thirds are used for AFM analysis of the fractions of each species and the number of monomers. The mutation experiments were conducted with starting templates of AB dimers and a pool of the AB:A:B:C:D monomers at a concentration of 0.1:1.6:1.6:1.6:1.6 nM (Fig. 3*B*). The refresh of monomers (A:B:C:D = 1.6:1.6:1.6:1.6 nM) was replenished into the system after each self-replication cycle. We conducted 15 cycles of self-replication and tracked the evolution of the AB and CD dimer composition using the AFM. Mutation started at the beginning of self-replication experiments, as mutated CD dimers were observed after the first cycle (Fig. 3*E* and *SI Appendix*, Fig. S5). The fraction of CD dimers was small at the beginning, but we observed more and more CD dimers through 15 cycles of self-replication, and the difference in the ratio of the two species got smaller (Fig. 3*D*). We further estimated the dimer composition after self-replication using the first-order master equations (*SI Appendix*, Eqs. **S1** and **S2**) with the initial composition, the mutation rate, and the same growth rate for both species. The calculated fraction of the two species fits well with the experimental data (Fig. 3*D*). Analytically, if two species have the same mutation rate, one to the other, then the two species would eventually equalize if they have the same competitiveness, the growth rate.

We conducted a similar self-replication using two species with different growth rates. The mechanism of mutation and photo-cross-linking was the same between AB and CD dimers but the competitiveness in the self-replication growth rate was largely determined by the recognition strands design. As illustrated in Fig. 4*A*, we changed the recognition strands design of AB dimer to the one-sided design with the maximum replication rate of 2. Thus, species AB has a lower growth rate than species CD, which still forms ladders and produces litters. We conducted the mutation experiments with the AB dimer as the only seed template and A, B, C, and D monomers at a concentration of 0.1:1.6:1.6:1.6:1.6 (Fig. 4*B*). Fresh monomers (A:B:C:D = 1.6:1.6:1.6:1.6 nM) were replenished after every

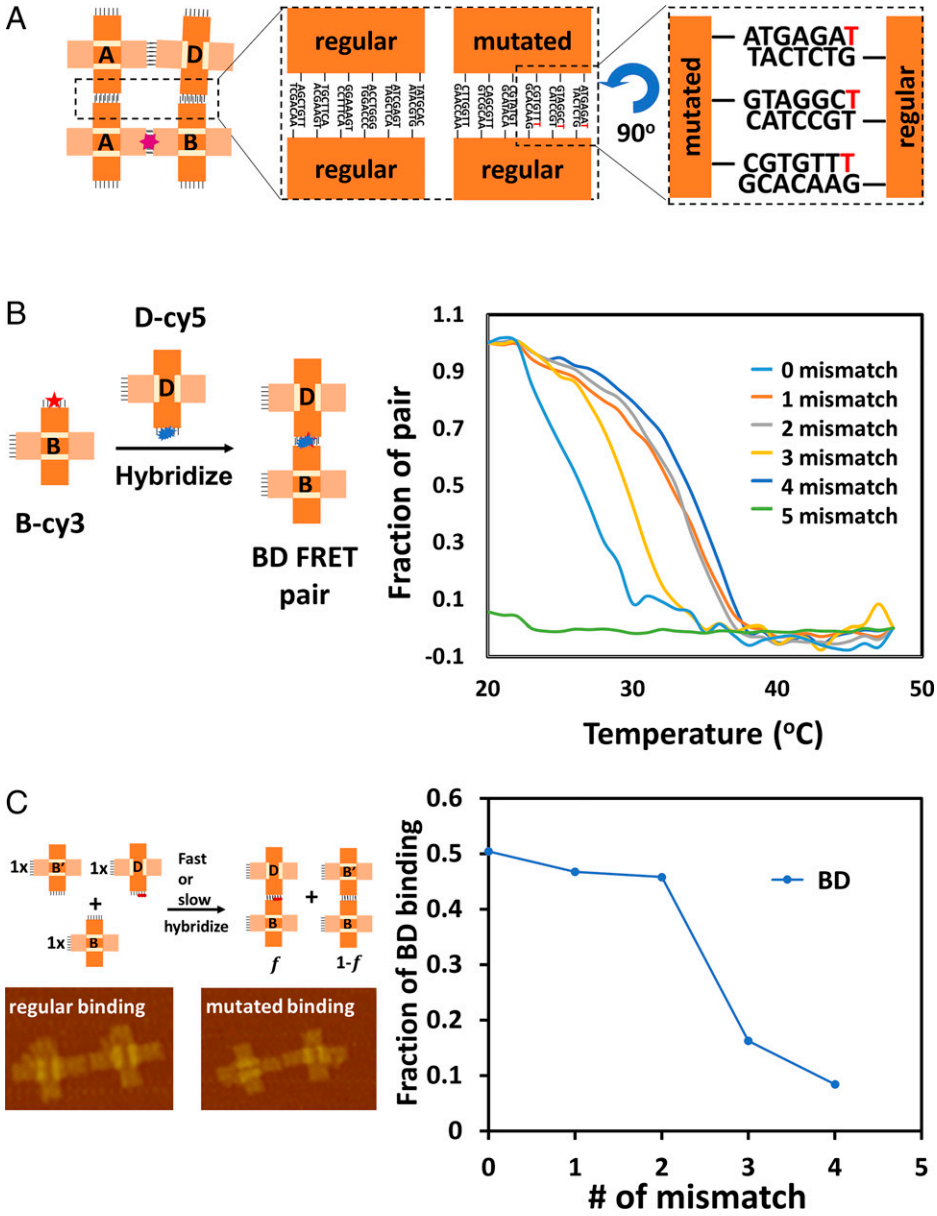

Fig. 2. (*A*) Schematics of the sticky-ends design for mutated self-assembly. The mismatch nucleotide (red) determines the mutation rate in the self-assembly. This schematic demonstrates three mismatches in the mutated hybridization. (*B*) Thermodynamic study of mutated self-assembly of B and D during annealing process through FRET. Schematics (*Left*) and hybridization curve (*Right*) of the vertical self-assembly between B–cy3 (donor) and D–cy5 (acceptor) from 48 °C to 20 °C. The hybridization curve shows that the melting temperature of mutated self-assembly decreases with more mismatch introduced. (*C*) The effect of mismatch in the selection of hybridization. (*Left*) Schematics of hybridization selection between B-B (regular binding without mismatch) and B-D (mutated binding with mismatch) at the equal amount through fast (1 h) annealing process. (*Right*) Fraction of mutated hybridization (B-D) over the number of mismatches by counting the dimer structure in the AFM images.

self-replication cycle. The agarose gel showed that the dimers increased every cycle and the growth rate increased from 1.6 to 2.5 after 13 replication cycles, indicating that the mutated CD dimers with the higher growth rate dominated the system (*SI Appendix*, Fig. S6 and Table S3). On the AFM images the mutant CD dimer fraction increased after each cycle (Fig. 4 *E* and *F* and *SI Appendix*, Fig. S7). In Fig. 4 *C* and *D* we plot the fraction of CD dimers and the amplification of AB and CD dimers vs. the number of cycles. Starting from zero the mutated CD dimers reached the same level as the AB dimers within only five cycles of self-replication. The mutants took over the system afterward and kept increasing their proportion until reaching a plateau after nine cycles (Fig. 4*C*).

The experimental data fit well with simulation results. Based on the self-replication rate from the gel analysis (*SI Appendix*, Table S4) and the experimental composition of two species (Fig. 4*C*), we calculated the amount of the AB and CD dimers after each cycle of self-replication. The logarithm of the AB and CD dimers can be well-fitted to a linear curve within the first eight cycles of self-replication, indicating the exponential growth of the two species even though their continued a small mutation rate from AB to CD and CD to AB. Since the growth rate is the only competitiveness in this artificial self-replication, the mutated CD dimers with a higher growth rate eventually dominated the system independent of the initial seed. As our system approaches saturation, the experiment deviates from the simple prediction. We

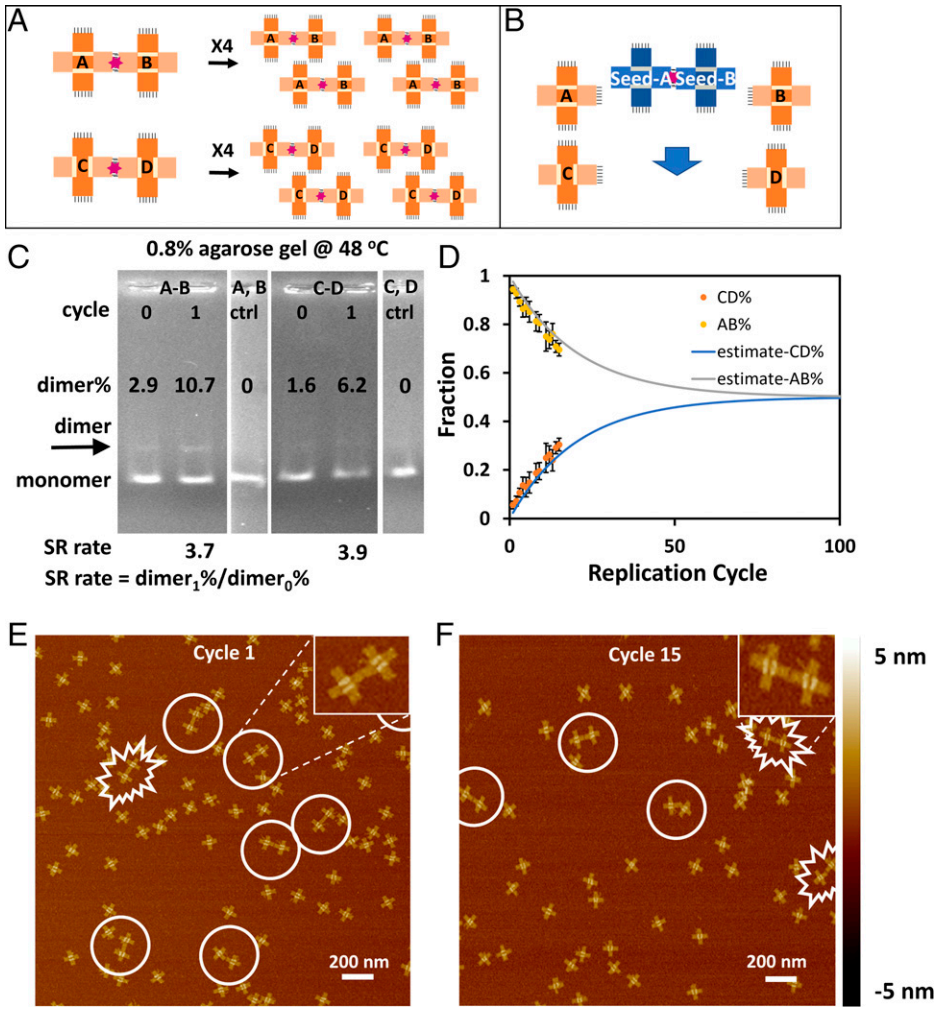

Fig. 3. (*A*) Schematic of two replication systems, A-B and C–D, with high replication rate using the ladder design. With the proper initial ratio between seed and monomer, the number of dimers can be multiplied by 4 (×4) after self-replication. (*B*) Schematic of the mutation experiment starting with all four monomers and only A-B seed dimer. Note: The mutated self-assembly rate from A-A to A-C is 16%. (*C*) When the seed:monomer ratio was about 1:32:32, a nondenaturing agarose gel (0.8%) shows the self-replication rate (SR rate) of A-B as 3.7 and that of C-D as 3.9, while the control experiment shows no dimer was formed without the seed. The gel was run at 48 °C. (*D*) The fraction of regular species (A-B) and mutated species (C-D) through 15 cycles of self-replication based on the counting of two species on AFM images. The solid line was the estimate of the species fraction based on the replication rate and the mutated self-assembly rate. (*E* and *F*) Representative AFM images of the sample after self-replication cycle 1 (*E*) and cycle 15 (*F*) show the change in the number of two species from seven AB and one CD after cycle 1 to three AB and two CD after cycle 15. The regular species are labeled with a circle and the mutated species are labeled with a 14-point explosion marker. The AFM sample are prepared at 48 °C to dehybridize the noncross-linked monomer. The 2.5- × 2.5-μm^2 representative AFM images were magnified from the 32- × 32-μm^2 whole image. The data in *D* come from imaging 874 "|| ||" and "= =" dimers from frames such as *E* and *F*.

attribute this difference to accumulation of parasite, sterile, nontemplated dimers which do not replicate according to our previous experiments (19). We allow for self-replication by adding monomers each cycle proportionate to the parent dimers and their growth rate. As shown in *SI Appendix*, Fig. S8 a nontemplated binding rate of 0.0007 dimers/monomer cycle well accounts for the experimental data in Fig. 4*C*.

Conclusion

We have developed an artificial system of DNA origami tiles of two species in which we can control the growth rates separately. Adding the ability of one species to mutate into the other, we have studied the evolution of the system where only one species is seeded. When growth rates are equal the system evolves to a steady state of equal populations. When one has the competitive advantage of faster growth it quickly becomes the dominant species, even when it only results from a mutation from the originally seeded and exponentially growing species. This is the expected result and a most elementary example of Darwinian evolution but here in an artificial self-replication system. Our system can be readily generalized to have many different types of mutations by adding E, F, G, H … monomer tiles with different sticky end sequences and with different growth rates depending on their rigidity, structure, and sensitivity to pH, ionic concentration, and other physical and chemical properties of their environment. It opens the door to the use of human-made systems, devices, and materials that evolve to have desired properties. In a given environment mutations allow the creation of a set of species and evolution picks the species which grows fastest in that environment, mimicking nature but with artificial constructs.

Materials and Methods

DNA Synthesis and Purification. Scaffold DNA M13mp18 was purchased from Bayou Biolabs. ^{CNV}K phosphoramidite was purchased from Glen Research. The DNA strands containing the ^{CNV}K were synthesized on an Applied Biosystems

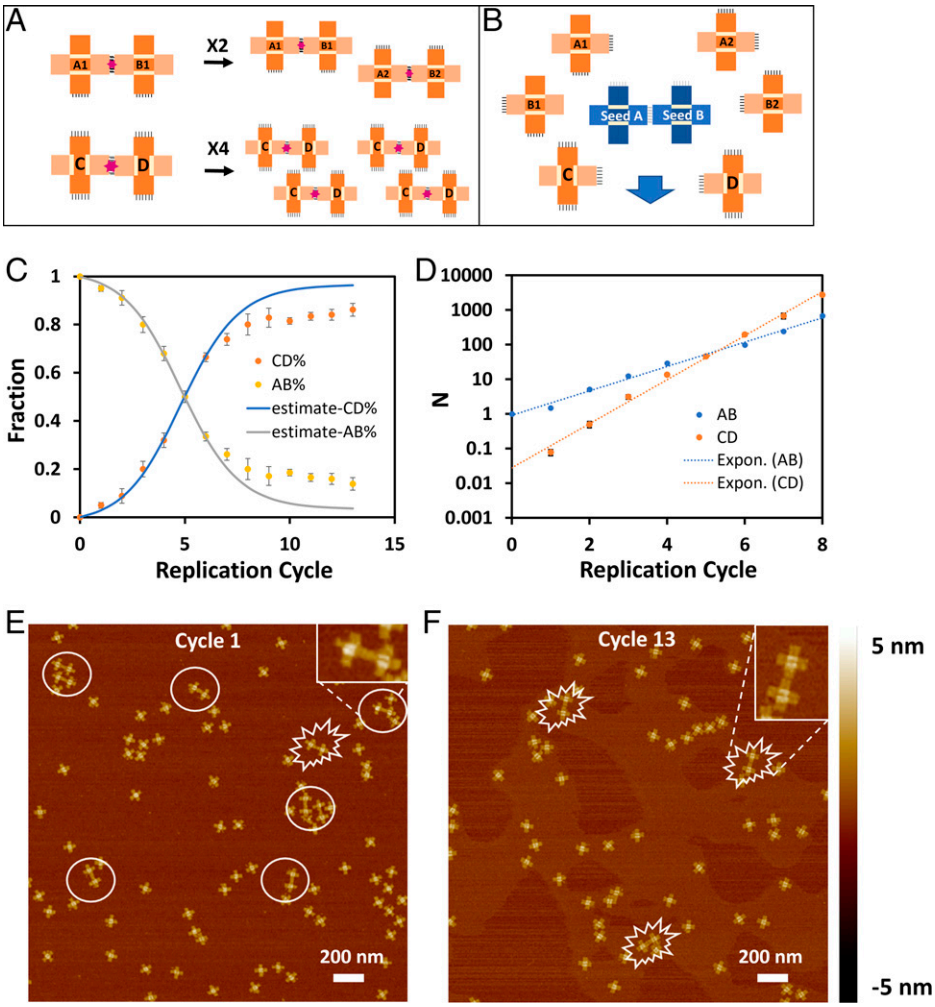

Fig. 4. (*A*) Schematic of two replication systems, A-B and C-D, with different replication rates. (*B*) Schematic of the mutation experiment starting with all four monomers and only A-B seed dimer. (*C*) The fraction of regular species (A-B) and mutated species (C-D) through 13 cycles of self-replication based on the counting of two species on AFM images. The solid line was the estimate of the species fraction based on the replication rate and the mutated self-assembly rate. (*D*) The natural logarithm numeral evolution of the two species through the first eight cycles of self-replication. (*E* and *F*) The representative AFM images of the sample after self-replication cycle 1 (*E*) and cycle 13 (*F*) show the change in the number of two species from five AB and one CD after cycle 1 to zero AB and three CD after cycle 13. The regular species are labeled with a circle and the mutated species are labeled with a 14-point explosion marker. The AFM sample are prepared at 48 °C to dehybridize the noncross-linked monomer. The 2.5- × 2.5-μm^2 representative AFM images were magnified from the 32- × 32-μm^2 whole image. The data in *C* come from imaging 1,635 "||||" and "=||" dimers from frames such as *E* and *F*.

394 DNA synthesizer. The remaining DNA strands were purchased from Integrated DNA Technology, Inc. The sticky-end strands were purified using denaturing polyacrylamide gel electrophoresis. The staples strands with dyes (cy3 and cy5) were purified by IDT using high-performance liquid chromatography.

Formation of Individual DNA Origami Tiles. Staple strands and M13mp18 scaffold DNA were mixed in 1× TAE/Mg^{2+} buffer (40 mM Tris·HCl, 20 mM acetic acid, 2.5 mM ethylenediaminetetraacetic acid, and 12.5 mM magnesium acetate, pH 8.0). The molar ratio of scaffold:staple strand was 1:8, and the final concentration of the scaffold DNA was 10 nM. The mixture was heated to 70 °C for 20 min and cooled to 20 °C at a rate of −7 °C/h in a thermocycling incubator. The resulting origami tiles were purified in 100K Millipore Amicon Ultra 0.5-mL centrifugal filters at 40 °C five times to remove the excess staple DNA strands. The weight concentration of the DNA origami was measured by IMPLEN NanoPhotometer Pearl using the double strands mode at 260 nm. The molar concentration was calculated by dividing the weight concentration over the molar mass of DNA origami (around 7,500 base pairs [bp] × 650 Da/bp).

Formation of Seed Dimer. For the three types of seed dimer origami tiles, the monomers of the same species were preheated to 53 °C for 30 min and then mixed at a 1:1 ratio. The mixture was cooled to 20 °C at a rate of −0.7 °C/h.

Self-Replication Cycling. Thirty microliters of solution containing seed dimers and monomer tiles was prepared at the following concentrations (in nanomolar):

1) Fig. 3*C*: seed AB:A:B = 0.1:3.2:3.2; seed CD:C:D = 0.1: 3.2: 3.2
2) Fig. 3*D*: seed AB:A:B:C:D = 0.1:1.6:1.6:1.6:1.6
3) Fig. 4: seed AB:A1:B1:A2:B2:C:D = 0.1:1.6:1.6:1.6:1.6:1.6:1.6
4) *SI Appendix*, Fig. S1*A*: seed AB:A1:B1:A2:B2 = 0.4:1.6:1.6:1.2:1.2
5) *SI Appendix*, Fig. S1*C*: seed AB:A:B = 0.2:3.2:3.2, 0.1:3.2:3.2, and 0.025:3.2: 3.2, respectively.

A 10-μL sample was taken out to quantify the initial dimer amount and the rest of the solution was covered with 50 μL silicone oil (HR3-415: Hampton Research) to prevent the evaporation-induced concentration change. The solution was heated to 48 °C for 30 min to break the vertical sticky-end hybridization and then annealed at 22 °C for 1 h for the seed-templated self-assembly. The sample was exposed to a 365-nm UV light-emitting diode (LED) (M365LP1c, power intensity 24 mW/mm^2; Thorlabs Inc.) at 22 °C for 20 min. A 10-μL sample was then extracted for AFM imaging and nondenaturing 0.8% agarose gel electrophoresis to determine the resulting amplified dimer amount. For the multicycle self-replication, an additional 20 μL of fresh monomers of the same concentration was transferred into the original tube before the next cycle of annealing and photo-cross-linking.

Gel Electrophoresis. A 0.8% agarose gel was prepared and immersed in the 1× TAE/Mg^{2+} buffer inside the gel electrophoresis box. Five-microliter samples were mixed with 1 μL nondenaturing tracking dye (1× TAE/Mg^{2+} buffer, 50% glycerol, and trace amount of bromophenol Blue and Xylene Cyanol FF). Gel was run at 4 to 5 V/cm at 48 °C for 3 h. The gel was immersed in the ethidium bromide solution for staining and rinsed with water to remove excess stain. The fluorescent gel image was processed using ImageJ to quantify the amount of the dimers and monomers to calculate the dimer percentage (dimer%). The growth rate of each self-replication cycle was calculated by dividing the dimer% after UV cross-linking over the dimer% before UV cross-linking. When there is no monomer replenishment, the dimer% before and after UV would be marked as cycle 0 and cycle 1, and the growth rate was calculated as dimer% (cyc1)/dimer% (cyc0).

AFM Imaging. AFM imaging was performed in peakForce mode in air for the self-replication cycling. Two to five microliters of a diluted sample was deposited on a clean mica surface (Ted Pella, Inc.) for 1 min. Unless specified, the sample and mica were incubated at 48 °C for 30 min and the deposition was conducted at 48 °C. The mica was then washed with 50 to 70 μL of double-distilled H_2O three times and subsequently dried using N_2. PeakForce in air mode was performed on the Nansocope V Multimode 8 scanning probe microscope (PeakForce QNM Software, ScanAsyst-HR accessory). Silicon nitride tips (ScanAsyst-Air; Bruker Nano, Inc.) were used for the Nanoscope V Multimode 8 SPM.

FRET Experiment. The FRET experiment was conducted using a Horiba PTI QuantaMaster 400 Fluorescent Spectrometer. Cy3 (donor) and Cy5 (acceptor) dye was modified on the vertical and horizontal sticky ends to make B-cy3 (donor), D-cy5 (acceptor), and cy3-FG-cy5 (donor acceptor). The concentration of B and D was 3.2 nM for the mutated vertical sticky end hybridization (Fig. 2*B*); the concentration of seed was 1.6 nM and the cy3-FG-cy5 tile was 3.2 nM for the ^{CNV}K-horizontal sticky-end hybridization (*SI Appendix*, Fig. S9). The sample solution was covered with silicon oil to prevent evaporation. For the thermodynamic study of vertical sticky-end hybridization (Fig. 2*B* and *SI Appendix*, Fig. S2), the sample was annealed from 20 °C to 48 °C, then back to 20 °C for three cycles. The ramping rate was 3 min/°C, and the fluorescent signal was measured at each degree. For the study of horizontal sticky end hybridization (*SI Appendix*, Fig. S9), the annealing temperature range was from 10 to 40 °C. The calculation method of the hybridization percentage can be found in our previous report (20).

Data Availability. All study data are included in the article and/or *SI Appendix*.

ACKNOWLEDGMENTS. This research has been primarily supported by Department of Energy (DOE) DE-SC0007991 to P.C., N.S., R.S., F.Z., and H.N. for initiation, design, analysis, and imaging. P.C. acknowledges support from the Center for Bio-Inspired Energy Sciences, an Energy Frontier Research Center funded by the DOE, Office of Sciences, Basic Energy Sciences, under Award DE-SC0000989, for initiation, DNA sequence design, preparation, and characterization confocal microscopy. R.S. and N.S. acknowledge partial support from NSF EFRI-1332411 and CCF-1526650 for laboratory supplies, under Award DMR-1420073 for synthesis and characterization of the DNA origami. R.S. and N.S acknowledge MURI W911NF-11-1-0024 from the Army Research Office and MURI N000140911118 from the Office of Naval Research for partial salary support. R.S. and N.S. acknowledge partial support from RGP0010/2017 from Human Frontiers Science Program. R.S. and N.S. acknowledge partial support from DOE DE-SC0007991 for DNA synthesis and partial salary support. The authors are grateful for shared facilities provided through the MRSEC program of the NSF under Award DMR-1420073.

1. P. W. K. Rothemund, Folding DNA to create nanoscale shapes and patterns. *Nature* **440**, 297–302 (2006).
2. S. M. Douglas *et al.*, Self-assembly of DNA into nanoscale three-dimensional shapes. *Nature* **459**, 414–418 (2009).
3. E. S. Andersen *et al.*, Self-assembly of a nanoscale DNA box with a controllable lid. *Nature* **459**, 73–76 (2009).
4. F. Zhang *et al.*, Complex wireframe DNA origami nanostructures with multi-arm junction vertices. *Nature* **10**, 779–784 (2015).
5. T. Gerling, K. F. Wagenbauer, A. M. Neuner, H. J. S. Dietz, Dynamic DNA devices and assemblies formed by shape-complementary, non-base pairing 3D components. *Science* **347**, 1446–1452 (2015).
6. W. Sun *et al.*, Casting inorganic structures with DNA molds. *Science* **346**, 1258361 (2014).
7. W. Liu, H. Zhong, R. Wang, N. C. Seeman, Crystalline two-dimensional DNA-origami arrays. *Angew. Chem. Int. Ed. Engl.* **50**, 264–267 (2011).
8. R. Iinuma *et al.*, Polyhedra self-assembled from DNA tripods and characterized with 3D DNA-PAINT. *Science* **344**, 65–69 (2014).
9. F. Zhou *et al.*, 3D freestanding DNA nanostructure hybrid as a low-density high-strength material. *ACS Nano* **14**, 6582–6588 (2020).
10. M. Y. Ben Zion *et al.*, Self-assembled three-dimensional chiral colloidal architecture. *Science* **358**, 633–636 (2017).
11. A. Kuzyk *et al.*, A light-driven three-dimensional plasmonic nanosystem that translates molecular motion into reversible chiroptical function. *Nat. Commun.* **7**, 10591 (2016).
12. H. T. Maune *et al.*, Self-assembly of carbon nanotubes into two-dimensional geometries using DNA origami templates. *Nat. Nanotechnol.* **5**, 61–66 (2010).
13. H. Pei *et al.*, Organizing end-site-specific SWCNTs in specific loci using DNA. *J. Am. Chem. Soc.* **141**, 11923–11928 (2019).
14. S. Zhao *et al.*, Efficient intracellular delivery of RNase A using DNA origami carriers. *ACS Appl. Mater. Interfaces* **11**, 11112–11118 (2019).
15. T. Wang *et al.*, Self-replication of information-bearing nanoscale patterns. *Nature* **478**, 225–228 (2011).
16. R. Schulman, B. Yurke, E. Winfree, Robust self-replication of combinatorial information via crystal growth and scission. *Proc. Natl. Acad. Sci. U.S.A.* **109**, 6405–6410 (2012).
17. T. Li, K. C. Nicolaou, Chemical self-replication of palindromic duplex DNA. *Nature* **369**, 218–221 (1994).
18. J. Kim, J. Lee, S. Hamada, S. Murata, S. Ha Park, Self-replication of DNA rings. *Nat. Nanotechnol.* **10**, 528–533 (2015).
19. X. He *et al.*, Exponential growth and selection in self-replicating materials from DNA origami rafts. *Nat. Mater.* **16**, 993–997 (2017).
20. R. Zhuo *et al.*, Litters of self-replicating origami cross-tiles. *Proc. Natl. Acad. Sci. U.S.A.* **116**, 1952–1957 (2019).
21. M. E. N. Majerus, Industrial melanism in the peppered moth, *Biston betularia*: An excellent teaching example of Darwinian evolution in action. *Evo. Edu. Outreach* **2**, 63–74 (2009).
22. M. Eigen, P. Schuster, *The Hypercycle: A Principle of Natural Self-Organization* (Springer Science & Business Media, 2012).
23. Y. Yoshimura, K. Fujimoto, Ultrafast reversible photo-cross-linking reaction: Toward in situ DNA manipulation. *Org. Lett.* **10**, 3227–3230 (2008).